Cholesterol metabolism

MOLECULAR AND CELLULAR BIOLOGY, May 2009, p. 2716–2729 Vol. 29, No. 10
0270-7306/09/$08.00+0 doi:10.1128/MCB.01638-08

Cholesterol Metabolism: the Main Pathway Acting Downstream of Cytochrome P450 Oxidoreductase in Skeletal Development of the Limb▽†

Katy Schmidt,[1]* Catherine Hughes,[2] J. A. Chudek,[3] Simon R. Goodyear,[4] Richard M. Aspden,[4] Richard Talbot,[5] Thomas E. Gundersen,[6] Rune Blomhoff,[6] Colin Henderson,[2] C. Roland Wolf,[2] and Cheryll Tickle[1]*

Division of Cell and Developmental Biology, Wellcome Trust Biocentre, University of Dundee, Dundee DD1 5EH, United Kingdom[1]; Cancer Research UK, Molecular Pharmacology Unit, Biomedical Research Center, Ninewells Hospital and Medical School, Dundee DD1 9SY, United Kingdom[2]; Division of Biological Chemistry, Wellcome Trust Biocentre, University of Dundee, Dundee DD1 5EH, United Kingdom[3]; Division of Applied Medicine, IMS Building, Foresterhill, Aberdeen AB25 2ZD, United Kingdom[4]; Roslin Institute, Edinburgh EH25 9PS, United Kingdom[5]; and Institute of Basic Medical Sciences, University of Oslo, Oslo, Norway[6]

Received 21 October 2008/Returned for modification 14 December 2008/Accepted 21 February 2009

Cytochrome P450 oxidoreductase (POR) is the obligate electron donor for all microsomal cytochrome P450 enzymes, which catalyze the metabolism of a wide spectrum of xenobiotic and endobiotic compounds. Point mutations in *POR* have been found recently in patients with Antley-Bixler-like syndrome, which includes limb skeletal defects. In order to study P450 function during limb and skeletal development, we deleted *POR* specifically in mouse limb bud mesenchyme. Forelimbs and hind limbs in conditional knockout (CKO) mice were short with thin skeletal elements and fused joints. *POR* deletion occurred earlier in forelimbs than in hind limbs, leading additionally to soft tissue syndactyly and loss of wrist elements and phalanges due to changes in growth, cell death, and skeletal segmentation. Transcriptional analysis of E12.5 mouse forelimb buds demonstrated the expression of P450s involved in retinoic acid, cholesterol, and arachidonic acid metabolism. Biochemical analysis of CKO limbs confirmed retinoic acid excess. In CKO limbs, expression of genes throughout the whole cholesterol biosynthetic pathway was upregulated, and cholesterol deficiency can explain most aspects of the phenotype. Thus, cellular POR-dependent cholesterol synthesis is essential during limb and skeletal development. Modulation of P450 activity could contribute to susceptibility of the embryo and developing organs to teratogenesis.

The P450 system is best characterized for its role in the metabolism and detoxification of environmental chemicals in adult liver (57). However, some subfamilies of P450 enzymes also have a pivotal role in metabolizing endogenous compounds such as hormones and fatty acids (4, 63). Cytochrome P450 oxidoreductase (POR) is the obligate electron donor for all microsomal cytochrome P450 enzymes (Cyps) and, in the absence of POR, these enzymes are catalytically inactive (3). There are more than 100 P450 enzymes in mice and over 50 in humans, and the particular profiles of P450s, many of which are polymorphic, determine an individual's response to drugs (58, 59). Surprisingly, however, rather little is known about the function of these enzymes in embryonic development, although the recent discovery of point mutations in *POR* in patients with Antley-Bixler-like syndrome is direct evidence of their importance during human development (27, 29).

Several studies have shown that *POR* and genes encoding P450 enzymes are expressed in mouse embryos. *POR* expression has been detected from preimplantation stages onward (81), while the most comprehensive studies of expression of cytochrome P450s have revealed that genes encoding several of these enzymes are temporally regulated over four stages of development (13, 14); temporal regulation has also been shown for *Cyp1A1* in more detail (7). These P450 studies, however, were based on reverse transcription-PCR and did not give any information about tissue localization.

Deletion of individual P450 genes in mice has uncovered some essential developmental roles. Members of the Cyp26 subfamily of P450s are involved in degrading retinoic acid, an important signal in the development of many parts of the embryo. Retinoic acid concentration in embryos is regulated via a feedback mechanism (19, 66), with production and degradation of retinoic acid taking place in complementary domains (83). Deletion of *Cyp26* genes leads to increased levels of retinoic acid and developmental defects (70, 96). In addition, cholesterol, synthesized by Cyp51 and metabolized by other Cyp family members to produce steroid hormones and vitamin D (56, 65), is known to be essential for normal development (69).

Another approach that has been taken to understand the essential role of the P450 system in embryonic development has been the deletion of *POR* and, as a consequence, the removal of all microsomal P450 function. This approach avoids problems with multiplicity and functional redundancy of Cyp enzymes. *POR* deletion in mice leads to elevated retinoic acid levels and embryonic lethality prior to organogenesis and limb

* Corresponding author. Mailing address for Cheryll Tickle: Department of Biology and Biochemistry, University of Bath, Claverton Down, Bath BA2 7AY, United Kingdom. Phone: 44-(0)1225-385015. Fax: 44-(0)1225-386779. E-mail: cat24@bath.ac.uk. Mailing address for Katy Schmidt: Department of Biochemistry, University of Bristol, University Walk, Bristol BS8 1TD, United Kingdom. Phone: 44-(0)117 -3312163. Fax: 44-(0)117-3312168. E-mail: k.schmidt@bristol.ac.uk.

† Supplemental material for this article may be found at http://mcb.asm.org/.

▽ Published ahead of print on 9 March 2009.

initiation, implicating retinoic acid metabolism as the major P450 pathway (64, 67) downstream of POR function in the early embryo. When retinoic acid levels were reduced either by feeding *POR*-deficient mice with a retinoid-deficient diet (64) or, genetically, by crossing them with mice haploinsufficient for the retinoic acid-generating enzyme Raldh2 (67), embryonic development improved, some $POR^{lox/lox}$; $Raldh2^{lacZ/+}$ embryos surviving until embryonic day 13.5 (E13.5). Knockout of the membrane-binding domain of POR (75) also resulted in longer survival.

We have focused here on the P450 system in limb development. The limb is one of the best-studied organ systems in vertebrate embryos and a well-known target for teratogens. *POR* has been reported to be expressed in E12.5 mouse limb mesenchyme and later, at E13.5, at high levels in joint-forming regions and perichondrium (43). Limb buds in $POR^{lox/lox}$; $Raldh2^{lacZ/+}$ embryos surviving until E13.5 had anteroposterior patterning defects (68), and limb buds in embryos in which the membrane domain of POR was knocked out were described as abnormal (75). Furthermore, some patients with *POR* mutations have defects in the limb skeleton (29). We generated a conditional knockout mouse line by crossing *Prx1-Cre* mice (51) to mice in which both alleles of *POR* are flanked by *loxP* sites (36). The *Prx1-Cre* mouse line has been widely used to knock out genes specifically in limb bud mesenchyme cells, which give rise to the skeleton and other connective tissues (1, 15, 49, 84). Gene knockout has been reported to occur at E9.5 in forelimb buds but slightly later in hind limb buds (51). This conditional approach creates a peripheral dysfunction, thus avoiding the embryonic lethality of a systemic *POR* knockout.

We found that *POR* deletion in mouse limb buds leads to defects in both patterning and skeletogenesis. Microarray analysis suggested the involvement of P450 pathways participating in retinoic acid, cholesterol, and arachidonic acid metabolism. All trans-retinoic acid was elevated, while cholesterol was reduced in CKO limbs. Most aspects of the *Prx1-Cre*; $POR^{lox/lox}$ limb phenotype can be explained by cholesterol deficiency.

MATERIALS AND METHODS

Animal husbandry. $POR^{lox/lox}$ mice (C57BL/6; N6) were crossed with a transgenic mouse line [Tg(Prrx1-Cre)1Cjt] expressing *Cre* recombinase under the control of the *Prx1* promoter (*Prx1-Cre*) on a C57BL/6 background (51). *Prx1-Cre*; $POR^{lox/+}$ offspring were backcrossed with $POR^{lox/lox}$ mice to generate limb-specific *POR* knockout (*Prx1-Cre*; $POR^{lox/lox}$) and control (*wildtype*; $POR^{lox/lox}$) mice. Presence of the *Prx1-Cre* transgene was determined by PCR using 5′-ACCTGAAGATGTTCGCGATTATCT-3′ and 5′-ACCGTCAGTACGTGAGATATCTT-3′. The floxed status of the *POR* gene was determined by PCR as previously described (36).

All mice were maintained under standard animal house conditions, with free access to food and water, and 12-h/12-h light-dark cycle. Mice were fed ad libitum on standard Rat & Mouse #1 maintenance diet or, alternatively, on special diets: a vitamin A-deficient (VAD) diet, a diet supplemented with 2% (wt/wt) cholesterol, or a combination of the two (Special Diets Services, Witham, Essex, United Kingdom). All mouse work was carried out in accordance with the Animal Scientific Procedures Act of 1986 and after local ethical review.

Scanning electron microscopy, micro-computed tomography (μCT), and micro-magnetic resonance imaging (μMRI). For scanning electron microscopy, E13.5 embryos were fixed in 2.5% glutaraldehyde at 4°C overnight, postfixed in 1% OsO_4 in cacodylate buffer, dehydrated in graded ethanol, placed in acetone, critically point dried, and sputter coated with gold/palladium. Forelimbs were dissected off and viewed on a Philips XL30 emission scanning electron microscope.

μCT was carried out by using a Skyscan 1072 X-ray microtomograph (Skyscan, Aartselaar, Belgium). Paraformaldehyde-fixed forelimbs were wrapped in Parafilm (American National Can, Chicago, IL) to prevent dehydration and mounted in the μCT vertically with the proximal end uppermost. Prior to scanning, the magnification was adjusted so the larger paw (from control) was contained within the field of view. This magnification was then maintained while scanning CKO limbs. The μCT scanner settings were as follows: pixel size, 7.32 μm; source, 50 kV/197 μA; rotation, 180°; rotation step, 0.68°; exposure time, 6 s; gain, 1.0; averaging, 1; flat field correction, on; random movement, 10; and filter, Al 0.5 mm.

Data for the μMRI images showing all tissue types were collected using a standard three-dimensional (3D) spin-echo sequence. 3D surface-rendered images were produced showing both the surface of the limb and the distribution of lipid within. A second acquisition sequence that suppressed the lipid signal was used to confirm the identification of the lipid. The data for images were accumulated on a Bruker Avance FT nuclear magnetic resonance spectrometer with a 7.1T wide bore vertical magnet resonating at 300 MHz for ^{1}H. The spectrometer was fitted with a Bruker microimaging accessory and probe equipped with a 25-mm birdcage resonator. The data were acquired using pulse sequences from the Bruker Paravision library (m_se3d, 3D spin-echo; m_suppress, 3D spin-echo with lipid suppression). For all samples, the probe was tuned and the magnet was shimmed before data acquisition. Four acquisition sequences were collected and averaged to improve the signal-to-noise ratio and remove artifacts. The acquisition parameters were as follows: matrix size, 256 by 256 by 256; field of view, 30.0 by 30.0 by 30.0 mm; and voxel dimensions, 120 by 120 by 120 μm. Imaging data were Fourier transformed, and then transferred to a PC for final visualization using AMIRA imaging software (Mercury Computer Systems, Inc., TGS unit, Whyteleafe, United Kingdom). A series of images was acquired using a range of acquisition parameters; images described here were acquired using a T_R/T_E of 300/25 ms. The AMIRA software allowed construction of pseudo 3D surface rendered images, which could be viewed from any angle.

Western blotting, immunohistochemistry, and skeletal staining. POR detection in whole-limb protein extracts was carried out with a polyclonal antibody raised to human POR (35). For anti-pH3 staining, sections were blocked with 10% fetal calf serum–1% bovine serum albumin in phosphate-buffered saline, incubated with primary antibody (1:100; Upstate, New York, NY) and detected with anti-rabbit-Alexa 488 (1:200; Molecular Probes, The Netherlands). Fluorescent images were taken with a Genoptic C14 camera on a Leica MZ Fluo3 microscope and processed with Openlab 4.1 and Adobe Photoshop CS2. Anterior of the limb bud is up and posterior is down in all images. Samples for histology were fixed in 4% paraformaldehyde for several days and processed according to standard staining protocols. Alcian Blue and Alizarin Red staining for cartilage and bone, respectively, was carried out as published previously (54), and limbs were measured under a binocular microscope with a vernier caliper.

TUNEL stain and in situ hybridization. TUNEL (terminal deoxynucleotidyltransferase-mediated dUTP-biotin nick end labeling) staining was performed according to the manufacturer's instructions on 14-μm frozen sections (in situ cell death detection kit fluorescein; Roche, Germany).

Whole-mount in situ hybridizations were carried out as described previously (67). Riboprobes were either cloned or kindly provided by Se-Jin Lee (*GDF5*), Robert Hill (*Msx2*), Klaus van de Mark (*Col2A* and *Col10*), Michael Wegner (*Ihh* and *Sox9*), Tomoko Iwata (*Patched1*), Andrea Vortkamp (*Gli1*), Brigid Hogan (*FoxC1*), Pascal Dollé (*Raldh2*), and Denis Duboule (*HoxD* probes). Images were taken and processed as described above. In situ hybridizations were carried out on three independent samples with little variability in the results, unless stated otherwise.

Whole-mount limb buds of *Cyp26B1* and *Raldh2* in situ hybridization experiments were processed and scanned by using optical projection tomography (74). 3D reconstruction of data was performed using AMIRA software.

Retinoid and sterol quantification. After genotyping, forelimb and hind limb buds of four E12.5 embryos were pooled separately to give single samples for forelimb buds and hind limbs, respectively. Pools were made from both normal and CKO embryos. Pooled limb buds (three pools) were homogenized in ice-cold phosphate-buffered saline with a motorized homogenizer (Pro Scientific, Inc., Oxford, CT), and retinoids were extracted with ice-cold 2-propanol containing ^{13}C-labeled all-trans retinoic acid (atRA) as an internal standard. An aliquot was injected into a 4000 Q TRAP LC-MS/MS instrument with APCI ionization (Applied Biosystems, California). The liquid chromatography-mass spectrometry conditions were as described previously (33), except that the separating column was an ABZ Plus (75 by 3 mm [inner diameter], 3-μm particles; Supelco, Pennsylvania). The entire procedure was performed under red light.

For sterol quantifications, left and right limb buds of E13.5 genotyped embryos were pooled to give single samples for forelimbs and hind limbs, respectively.

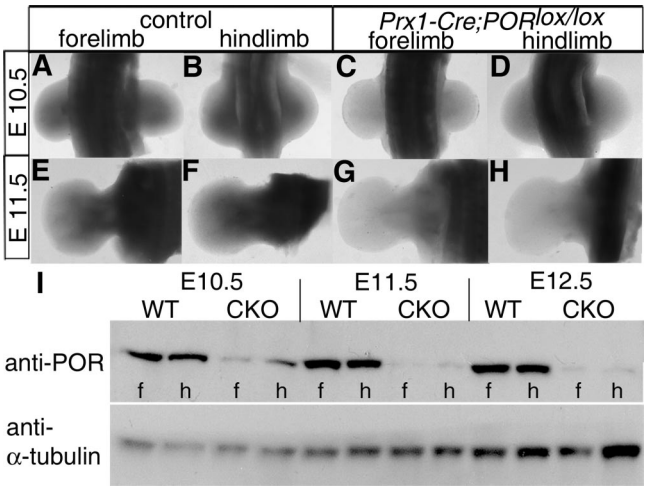

FIG. 1. Timing of *POR* knockout in limb buds of *Prx1-Cre*; *POR*$^{lox/lox}$ mice. In situ hybridization with a *POR*-specific probe on limb buds at E10.5 (A to D) and E11.5 (E to H). No signal was detected in CKO forelimb buds at E10.5 (compare panels A and C). POR deletion in hind limb buds occurs later at E11.5 (compare panels F and H). (I) Detection of POR protein in whole-limb protein extracts. POR protein was markedly reduced in E10.5 forelimb buds of CKO mice and undetectable at E11.5 in forelimb buds but faintly present in hind limb buds. α-Tubulin was used as a loading control. Representative images of two independent Western blot analyses are shown.

Sample preparation and enzymatic assays were performed according to the manufacturer's instructions (cholesterol quantification kit; Biovision, California).

For lipid analysis, tissue samples were prepared, weighed, and frozen on dry ice-ethanol. The lipid extraction method was adapted from that of a previous study (28) and carried out at the Mylnefield Lipid Analysis, Scottish Crop Research Institute, Invergowrie, United Kingdom. Briefly, chloroform–methanol–0.88% KCl (2:1:0.8 [vol/vol/vol]) was used for extraction, and the samples were washed with 0.88% potassium chloride-methanol (1:1 [vol/vol]). Oil content was calculated as an average of seven animals each and is expressed as a percentage from milligrams of oil per gram of tissue. For standard esterification, followed by gas chromatography, the American Oil Chemist Society official method ("Ce1b-89: Fatty Acid Composition by GLC, Marine Oils") was used. Mean values (three mice each) in percentages are given for cholesterol and lathosterol, with total sterol normalized to 100%.

Microarray analysis. Total RNA was extracted with TRIzol (Life Technologies, United Kingdom) according to the manufacturer's guidelines, except for the addition of 1 μl of linear acrylamide (Ambion, Inc., Texas) at precipitation, from pooled, genotyped E12.5 forelimb buds (four limb buds per pool). Five pools of control and five pools of CKO forelimb total RNA were prepared. Microarray analysis was carried out using standard protocols on Genechip Mouse 430 2.0 arrays (Affymetrix, United Kingdom). Amplified RNA was prepared from 5 μg of total RNA by using a GeneChip 3′ expression one cycle target labeling kit (Affymetrix) according to the manufacturer's recommendations. After overnight hybridization, arrays were processed using the Affymetrix fluidics station. Obtained images were processed with GCOS software, and the resulting CEL files were analyzed. Normalization of experimental data was done with Expression Console software (Affymetrix) using the PLIER algorithm.

Statistical analysis was carried out using the LIMMA (76) module in Bioconductor software (31). Differences between CKO and the control condition were examined by a modified *t* test, where the LIMMA eBayes correction was used to produce a moderated T-statistic, thereby shrinking estimated sample variances toward a pooled estimate, resulting in far more stable inference. The top 50 transcripts with the lowest false discovery rate were annotated using NetAffx website (http://www.affymetrix.com/analysis/index.affx) and subjected to pathway analysis with GenMAPP software (18). The complete data set is available at http://www.ebi.ac.uk/arrayexpress (E_TABM_367).

RESULTS

Conditional deletion of *POR* leads to limb malformations. In order to investigate POR function specifically in the developing limb bud and skeleton, we generated a conditional knockout mouse line, *Prx1-Cre*; *POR*$^{lox/lox}$ (CKO), by crossing *Prx1-Cre* mice (51) to mice with both alleles of *POR* flanked by *loxP* sites (36). We monitored POR knockout at both transcript and protein level in limb buds of *Prx1-Cre*; *POR*$^{lox/lox}$ embryos (Fig. 1). *POR* transcripts were absent and POR protein was moderately reduced at E10.5 and undetectable at E11.5 in forelimb buds (compare Fig. 1C to A; Fig. 1I), whereas, in hind limb buds, POR transcripts and protein were present at E10.5, and the protein was still faintly detectable at E11.5 (compare Fig. 1H to F; Fig. 1I).

The conditional deletion of *POR* during limb bud development resulted in limb malformations. In 7 day *Prx1-Cre*; *POR*$^{lox/lox}$ mice, the limbs were clearly abnormal (Fig. 2A), with forelimbs being much shorter and more malformed than hind limbs (57% of the length of control forelimbs and 79% of

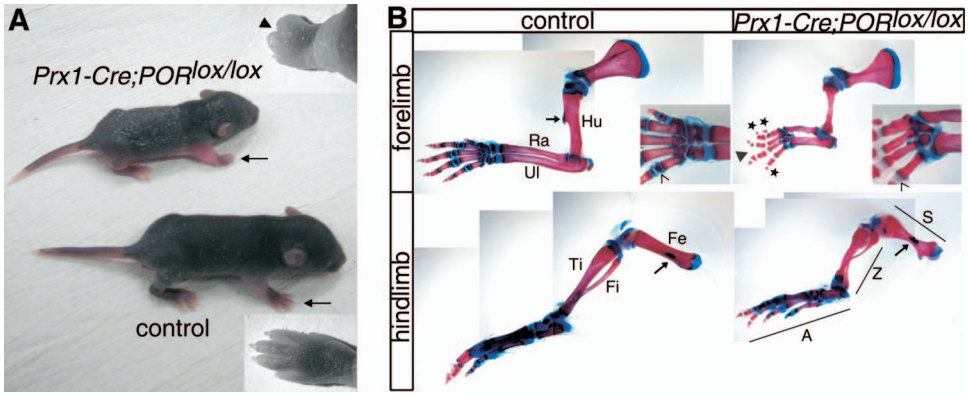

FIG. 2. Phenotypic characterization of 1-week-old *Prx1-Cre*; *POR*$^{lox/lox}$ forelimbs and hind limbs. (A) External view of CKO mouse and control littermate. Insets show dorsal view of forepaws; an arrowhead indicates splayed digits. Note the shorter forelimbs (arrowed) and overall size reduction. (B) Cartilage (Alcian Blue) and bone (Alizarin Red) staining of forelimbs and hind limbs. CKO forelimbs are shorter and have only two carpal bones (compare insets), no secondary ossification centers (open arrowhead), and a reduced number of phalanges in digits 1, 2, and 5 (stars). Processes on humerus and femur (arrows) are missing or reduced. CKO forepaws show characteristic splaying of digits 3 and 4 (arrowhead). Abbreviations: A, autopod; Fe, femur; Fi, fibula; Hu, humerus; Ra, radius; S, stylopod; Ti, tibia; Ul, ulna; Z, zeugopod.

control hind limbs, respectively). This difference in severity of the defects is consistent with the difference in developmental timing of knockout with *POR* being deleted at an earlier stage in the forelimb compared to the hind limb. More detailed external examination of the forelimbs also revealed that the digits appeared stunted and fused except for a pronounced interdigital space between digits 3 and 4 (Fig. 2A, compare insets).

Skeletal preparations of the limbs of 7 day *Prx1-Cre*; $POR^{lox/lox}$ mice showed that all bones were short and misshapen in both forelimbs and hind limbs with forelimb elements again more affected than those in hind limbs (Fig. 2B; see Table S1 in the supplemental material for measurements of the lengths of individual bones in forelimbs and hind limbs and details of skeletal phenotype analysis). Long bones in the stylopod (upper part of the limb, i.e., humerus in forelimb and femur in hind limb; Fig. 2B) and zeugopod (middle part of the limb, i.e., radius and ulna in the forelimb and tibia and fibula in the hind limb, Z in Fig. 2B) were thinner. Processes on humerus and femur were reduced or absent (Fig. 2B), no secondary ossification centers were seen (Fig. 2B) and in the hind limbs, the fibula was very bent and tibia and fibula were not fused (Fig. 2B). In addition, joints, especially at the knee and elbow, were malformed and swollen and, in about half of the CKO forepaws, fusion of digits and joints was noted (see Table S1 in the supplemental material). No skeletal patterning defects were seen in CKO hind limbs, but in CKO forelimbs digits 1, 2, and 5 lacked one phalange each (Fig. 2B), and six out of eight carpal bones were absent, leaving most likely hamate and central carpal bones (Fig. 2B, compare insets). The characteristic splaying of digits 3 and 4 in the forelimb was also clear in the skeletal preparations (Fig. 2B).

Postnatal consequences of functionally inactivating POR in the limbs were monitored over 2 months. The growth of both forelimbs and hind limbs was impaired with the forelimb continuing to be more affected (see Table 1 in the supplemental material). Comparison of the mineralized tissue of CKO forepaws and those of control mice using μCT showed that all skeletal elements were much shorter and generally misshapen in the CKO (Fig. 3A and B). The interdigital space between digits 3 and 4 was still very marked. Joint fusion in the CKO was already apparent at 7 days in half the animals studied (see Table 1 in the supplemental material), and histological sections through phalangeal joints at 2 months showed hyperproliferation of articular cartilage and fusion across the synovial cavity (Fig. 3A and B, compare insets). In the soft tissue, a substantial increase in lipid in the CKO paws could be visualized with μMRI by separating water and lipid resonances (Fig. 3C and D). The spongy appearance of the tissue in histological sections of the proximal region of the CKO paws (Fig. 3F inset) and the higher levels of extractable oil from the samples (Fig. 3C and D, values on the bottom) confirmed the lipid accumulation. Comparison of normal and CKO in the interdigital region highlighted spongelike tissue in regions where muscle was normally present (see Fig. S1E and F in the supplemental material), suggesting that lipid has accumulated in muscle. Thus, at 2 months, functional inactivation of POR in the limb has led to continued reduction in longitudinal growth and lipid accumulation. Some of these changes could be secondary due to the lack of normal usage of the limb.

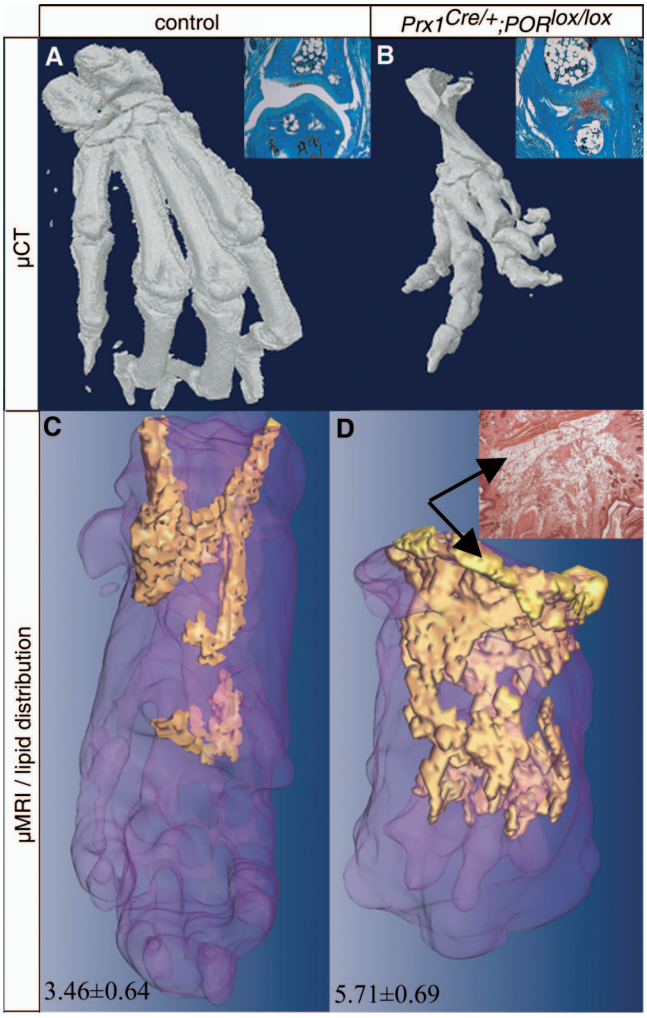

FIG. 3. Postnatal development of the phenotype. (A and B) μCT images of forepaws of 2-month-old mice. Dorsal view. Insets show histological sections through intraphalangeal joints. The CKO digit has malformed joints. (C and D) μMRI images of 2-month-old forepaws. A ventral view of the skeleton (darker purple) is shown; surface lipid deposits are rendered in yellow. The inset shows a histological section through a CKO paw confirming fat accumulation. Values given at the bottom are expressed as milligrams of extracted oil per gram of tissue (mean of seven mice each).

Embryonic development of forelimb and skeleton in conditional *POR* knockout mice. In order to identify critical events leading to changes in *Prx1-Cre*; $POR^{lox/lox}$ mice, we followed forelimb development during embryogenesis because *POR* is deleted earlier in forelimbs than in hind limbs (Fig. 1), and this leads to more marked skeletal defects and also to patterning defects (Fig. 2B). At E10.5 and E11.5, stages at which POR protein was markedly reduced or no longer detectable, respectively (Fig. 1I), no change in the size and shape of forelimb buds was observed (compare Fig. 1A to C and Fig. 1E to G). External inspection of E12.5 forelimb buds (Fig. 4A and B) also did not reveal major differences between control and *Prx1-Cre*; $POR^{lox/lox}$ embryos, although CKO paws were slightly stunted (Fig. 4B). Chondrogenic condensations were similar in both genotypes (data not shown). In contrast, at E13.5, exter-

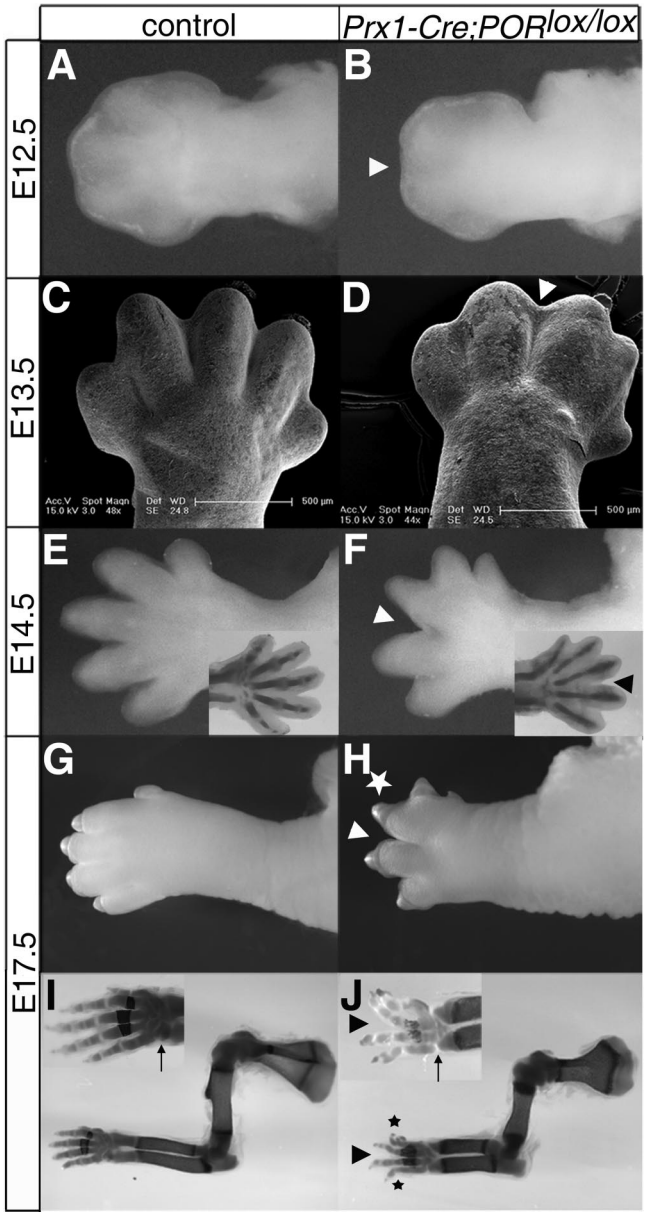

FIG. 4. External and skeletal phenotype of *Prx1-Cre*; *POR*$^{lox/lox}$ forelimb buds during embryogenesis. Embryonic ages are indicated on the left, and genotypes are indicated across the top. (A, B, E, F, G, and H) External dorsal views of fixed limb buds. At E12.5, CKO forelimbs are slightly stunted (arrowhead). (C and D) Scanning electron microscopy of E13.5 limb buds. Note the extended space between digits 3 and 4 (arrowheads) at E13.5 and E14.5 and the webbing in E17.5 CKO forelimbs (H, star). (E and F, insets) Cartilage (in dark gray) staining of E14.5 forelimb buds. (I and J) Cartilage and bone (in black) staining of E17.5 forelimbs. Note the deeper indentation between digits 3 and 4 at E13.5, E14.5, and E17.5 (arrowheads). At E17.5, two carpal bones are present (compare I and J, insets, arrows); posterior and anterior digits are less well developed (J, stars). Two or three limb buds were examined for each genotype with little or no variation; for E17.5 at least five limb skeletons were stained, and representative examples for each genotype are shown.

nal changes were immediately obvious in CKO forelimbs (Fig. 4C and D), and these were accentuated at E14.5 (Fig. 4E and F) and E17.5 (Fig. 4G and H). The outgrowth of digits in E14.5 *Prx1-Cre*; *POR*$^{lox/lox}$ limbs was reduced, as were indentations between digits 1, 2, and 3 and between digits 4 and 5, leading to soft tissue webbing especially involving digits 1, 2, and 3 (Fig. 4E and F). The indentation between digits 3 and 4, however, still developed so that these digits splayed apart. Alcian Blue staining at E14.5 also indicated delayed development of interphalangeal joints compared to control limbs (compare Fig. 4E and F, insets). In E17.5 CKO limbs, only digits 3 and 4 were clearly separated (Fig. 4H, arrowhead), and digits 1 to 3 appeared fused (Fig. 4H) due to soft tissue webbing (compare to Fig. 4G).

Skeletal preparations of E17.5 forelimbs not only showed the characteristic splaying of digits 3 and 4 in the CKO but also that stylo- and zeugopod were reduced in length and the humeral process was absent (Fig. 4I and J), while in the paw, only two carpal bones were present (Fig. 4J, inset, arrow, compare to 4I, inset), and the phalanges of digits 1, 2, and 5 were not fully segmented (Fig. 4J [compare to Fig. 4I]). Other postnatally obvious aspects of the phenotype had not yet appeared, in particular thinning of the long bones and swollen joints.

Soft tissue webbing in CKO forelimbs suggested impairment of interdigital cell death. In situ hybridizations on E12.5 limb buds for *Msx2* (71), a gene encoding a homeobox transcription factor associated with interdigital preapoptotic cells, showed that *Msx2* expression was markedly reduced in all interdigital spaces in CKO forelimbs except between digits 3 and 4 (compare Fig. 5A and B). TUNEL assays performed on sections of E13.5 limb buds confirmed reduced interdigital cell death between anterior digits although apoptosis appeared increased subapically (Fig. 5C and D). A decrease in apoptosis in CKO forelimb buds did not seem consistent with smaller paws, but overall proliferation was also reduced, as shown by immunostaining against phosphorylated histone H3 (compare Fig. 5E and F).

Another feature of *Prx1-Cre*; *POR*$^{lox/lox}$ forelimbs was failure to complete digit segmentation, leading to loss of a phalanx in digits 1, 2, and 5. In order to investigate phalanx segmentation, the expression of *GDF5*, a gene encoding a transforming growth factor β specifically expressed in joint-forming regions of developing limb buds (79, 80), was examined. No difference was detected at E12.5 between normal and CKO forelimb buds (Fig. 5G and H). At E13.5, the time at which it has been reported that *POR* is expressed at high levels in joint-forming regions (43), *GDF5* expression in CKO forelimbs was comparable to controls in digits 3 and 4 even though these were clearly reduced in length but compressed to one domain at both edges of the handplate (Fig. 5I and J). At E14.5, the handplate of *Prx1-Cre*; *POR*$^{lox/lox}$ limb buds appeared even more stunted and *GDF5* expression was generally increased even in interdigital regions, making it difficult to define the presumptive joints (Fig. 5K and L).

The patterning defect of missing wrist elements and phalanges prompted an investigation of expression of *HoxD11-HoxD13* genes known to be involved in development of skeletal elements in the distal limb (98, 99). No changes could be detected at either E12.5 or even at E13.5 when CKO forelimb buds were clearly misshapen (data not shown). Because patterning of the anterior and posterior autopods was most affected, *Tbx3*, normally expressed in anterior and posterior stripes in developing limb buds and implicated in digit speci-

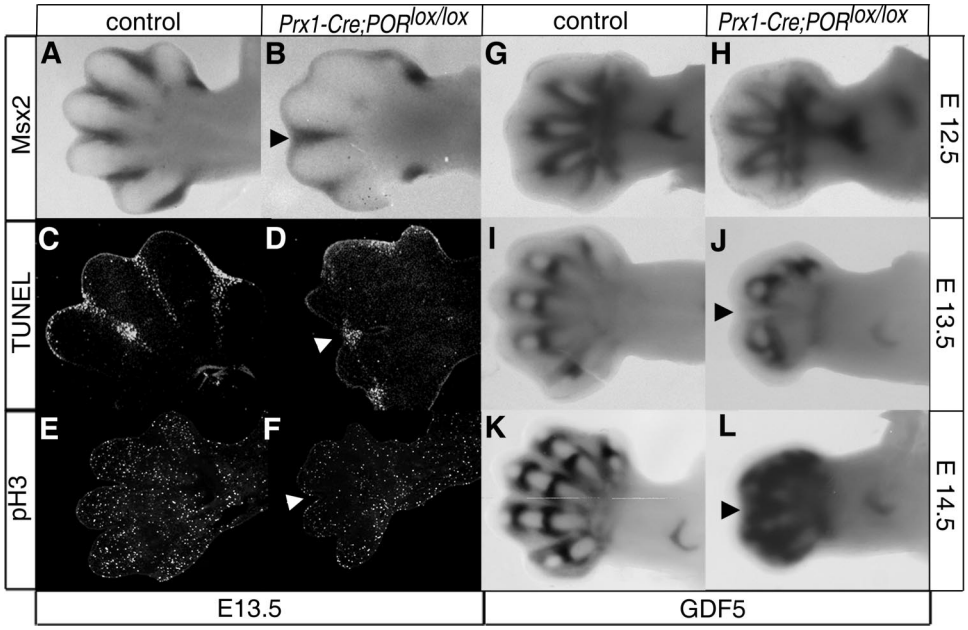

FIG. 5. Gene expression, proliferation, and apoptosis in *Prx1-Cre*; *POR*$^{lox/lox}$ forelimb buds. (A and B) In situ hybridization with a *Msx2*-specific probe at E12.5. Expression of *Msx2* is reduced in CKO limb buds (B), with the exception of the interdigital space between digits 3 and 4 matching the observed phenotype. (C and D) TUNEL stain on 14-μm cryosections of E13.5 limb buds indicating interdigital cell death. Note the reduction between digits 1 and 3 in the CKO sample. (E and F) Phospho-H3 immunofluorescence at E13.5 showing overall reduced proliferative activity in distal region of CKO limb buds. The fluorescence images (C to F) are representative of two experiments. Note the interdigital space between digits 3 and 4 (white arrowhead). (G to L) In situ hybridization with *GDF5*-specific probe. Embryonic ages indicated on right, and genotypes are indicated across the top. Note the stunted appearance of the CKO limb buds at E13.5 coinciding with a reduction in *GDF5* and more widespread expression of *GDF5* at E14.5.

fication (82, 86), was investigated, but again no difference in gene expression was seen in the CKO (data not shown).

Chondrogenesis of forelimb skeleton in *Prx1-Cre*; *POR*$^{lox/lox}$ mice. In order to investigate skeletal development in CKO forelimbs in more detail, we assessed expression of *Sox9* (Sry-related HMG box 9), a gene encoding a transcription factor required for mesenchymal condensation and chondrogenesis (1, 93). *Sox9* expression at E12.5 was very similar in forelimbs of both, control and CKO embryos consistent with Alcian Blue staining at this stage (data not shown) but by E13.5, *Sox9* expression appeared broader in digits of CKO forelimbs with less sharp boundaries and less definition around joint forming regions (compare Fig. 6A and B). Branching of digit 2 primordium was observed in one of three cases (Fig. 6B).

To study specific chondrogenic differentiation states, we examined the expression of *Collagen 2A* (*Col2A*), a transcriptional target of Sox9 in proliferating chondrocytes (60), and *Indian hedgehog* (*Ihh*) and *Collagen 10* (*Col10*), expressed in prehypertrophic and hypertrophic chondrocytes, respectively (22, 87). *Col2A* was expressed throughout all digit primordia similar to *Sox9* at both E12.5 (not shown) and E13.5 (compare Fig. 6A and B with Fig. 6C and D) with broader, less-well-defined expression in CKO limb buds; in one of three cases digit 2 was branched (Fig. 6D). Expression of *Col10* and *Ihh* was extended in the proximal region of middle digits, usually digits 3 and 4 but virtually absent in anterior and posterior digits (Fig. 6E to H). In contrast to all other gene expression patterns investigated, *Col10* and *Ihh* patterns appeared rather variable in that the size and shape of expression domains differed from embryo to embryo, e.g., more fan-shaped in one and more rod-shaped and shorter in another.

Microarray analysis. In order to gain insights into how the phenotype described above is related to function of POR and P450 enzymes during mouse limb development, we performed whole-genome expression analysis and evaluated the results of an average of five arrays per genotype. Transcriptional changes were investigated at E12.5, the time before marked morphological differences were obvious but at which there were already clear alterations in *Msx2* expression.

A total of 60 mouse *P450* genes have annotated probe sets on the 3′-expression array, and 14 out of these were found to be expressed in E12.5 forelimb buds (Fig. 7A; according to present calls in all five control arrays). For two, *Cyp2d22* and *Cyp20a1*, enzymatic substrates of their proteins are not yet known. The gene encoding the retinoic acid metabolizing enzyme, *Cyp26a1*, was expressed (Fig. 7A, green). Another member of this subfamily, Cyp26b1, was not represented on the array but is known to be expressed in limb buds at this stage (39, 70, 96). All other *P450*s present were involved in either arachidonic acid (Fig. 7A, black) or cholesterol (Fig. 7A, red) metabolism.

To identify gene expression changes in *Prx1-Cre*; *POR*$^{lox/lox}$ forelimb buds, a statistical analysis of all differentially expressed genes was performed. Surprisingly, expression of only 0.1% of genes represented on the array was found to be significantly changed with a low false discovery rate (Fig. 7B). These top 50 probe sets represent 39 different genes. As expected, *Msx2* was among downregulated transcripts (Fig. 7B

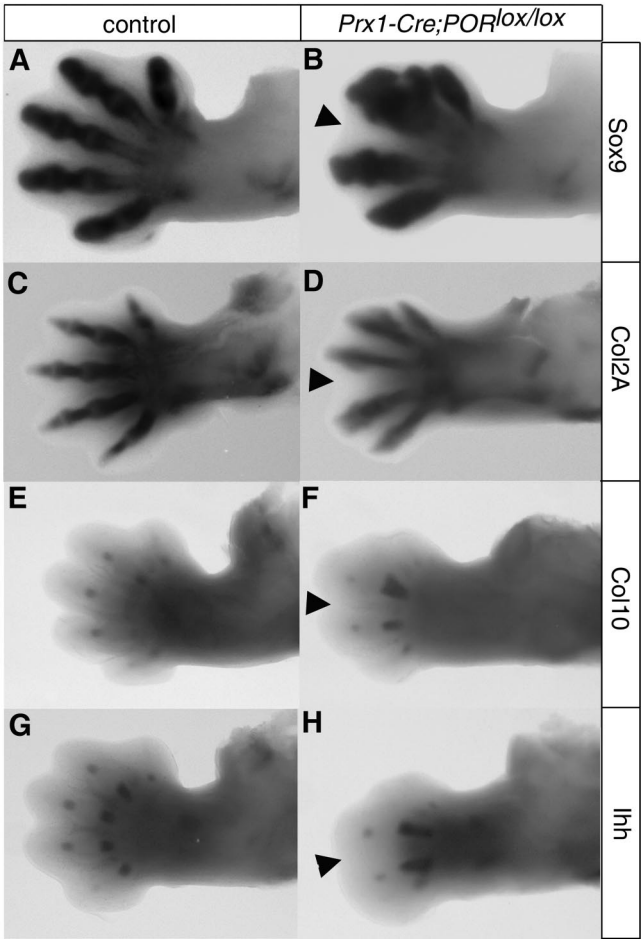

FIG. 6. Chondrogenesis in *Prx1-Cre*; $POR^{lox/lox}$ forelimb buds at E13.5. Whole-mount in situ hybridizations for *Sox9* (A and B), *Col2A* (C and D), *Col10* (E and F), and *Ihh* (G and H). (A and B) *Sox9* expression in CKO limb buds showed less sharp boundaries and no definitive joint-forming regions. (C and D) *Col2A* expressed in similar pattern to *Sox9*. Note the extended space between digits 3 and 4 in both expression patterns (arrowhead). (E and F) Expression of *Col10* in hypertrophic chondrocytes increased at base of presumptive digits 3 and 4 but reduced in other three digits in CKO. (G and H) *Ihh* expression in prehypertrophic chondrocytes resembles *Col10* pattern. The shapes and sizes—but not the locations—of both *Col10* and *Ihh* expression domains were variable. No variation was observed for control embryos.

and C, blue; see also Fig. 5B), while another transcription factor, *FoxC1*, was upregulated (Fig. 7B and C; blue). Subsequent in situ hybridizations for *FoxC1* (46) showed that this gene is expressed around forming digits at E12.5, and expression is elevated in CKO limb buds, in particular in the presumptive wrist region (Fig. 7D). The largest number of differentially expressed transcripts by far (23), however, was associated with cellular cholesterol homeostasis (Fig. 7B, red) and included transcripts encoding cholesterol synthesizing enzymes and sterol-sensing or transport proteins and the P450 enzyme, Cyp51 (see also Table S2 in the supplemental material). The gene encoding the retinoic acid metabolizing P450 Cyp26a1 was also on the list, together with the gene encoding the retinoic acid-synthesizing enzyme Raldh2 and transcription of these genes were up- and downregulated, respectively (Fig. 7B and C, green). The 12 remaining genes identified were either uncharacterized transcripts or unrelated to those described above.

Deletion of *POR* leads to excess retinoic acid. In the absence of POR, Cyp26 enzymes should be inactive, resulting in increased retinoic acid levels in CKO forelimb buds. It has previously been shown that genes encoding both retinoid-generating and retinoid-degrading enzymes are transcriptionally regulated by retinoic acid to maintain homeostasis (19, 66). The changes in transcript levels of retinoic acid metabolizing enzymes revealed by the microarray (Fig. 7B and C) therefore suggested the elevation of retinoic acid.

We confirmed changes in expression of genes involved in retinoic acid metabolism, *Cyp26b1* and *Raldh2*, in CKO limb buds at E11.5 and E12.5 using whole-mount in situ hybridization. *Cyp26b1* was chosen rather than *Cyp26a1* because both genes show essentially the same regulation (66), but *Cyp26b1* is better characterized in limb development (96), and we have previously shown an upregulation of *Cyp26a1* in POR-deficient limb buds (67). Only minor differences were detectable at E11.5 between control and *Prx1-Cre*; $POR^{lox/lox}$ forelimb buds for *Cyp26b1* (Fig. 8A and C), whereas *Raldh2* already appeared to be downregulated in CKO forelimbs (compare Fig. 8E and G). At E12.5, expression patterns for both genes agreed with the microarray results with *Cyp26b1* ectopically expressed in forelimbs (Fig. 8I and K), whereas *Raldh2* expression domains were smaller (Fig. 8M and O). There were no obvious differences in expression of either gene in hind limb buds at E11.5 or E12.5 (Fig. 8B, D, F, H, J, L, N, and P). A three-dimensional reconstruction of whole-mount in situ hybridization specimens at E12.5 (Fig. 8Q to T) showed that interdigital mesenchyme between forelimb digits 3 and 4 was the only domain with nonoverlapping expression *Cyp26b1* and *Raldh2*. It was development of this interdigital space that led to the characteristic splaying of digits 3 and 4 in CKO forelimbs (see for example, Fig. 2A and Fig. 4F and H).

Direct retinoid measurements in E12.5 limb buds showed elevated atRA in CKO forelimb buds, while the levels of atRA were similar in forelimb buds of control embryos and both CKO and control hind limb buds (Fig. 8U). The elevation of atRA resulted in around a 50% increase in the ratio of atRA to retinol in CKO forelimbs compared to control forelimbs in which the ratio was similar to that in both CKO and control hind limbs. From these results, we conclude that POR inactivation led to reduced retinoic acid degradation, resulting in accumulation of retinoic acid throughout E12.5 forelimb buds, except probably in the interdigital space between digits 3 and 4.

POR deletion leads to impaired cholesterol metabolism. The microarray results showed that genes encoding P450 enzymes involved in cholesterol metabolism, in particular *Cyp51*, are expressed in the handplate of E12.5 mouse forelimbs (Fig. 7A) and, since these require POR function for their activity, cholesterol homeostasis is predicted to be affected in CKO limb buds. It has been previously shown that reduced cholesterol leads to transcriptional upregulation of enzymes in the pathway (23). Strikingly, our microarray data showed that enzymes of almost the whole pathway, from acetyl coenzyme A all of the way down to cholesterol, were transcriptionally upregulated in CKO forelimbs (Fig. 7C and 9A, red), together

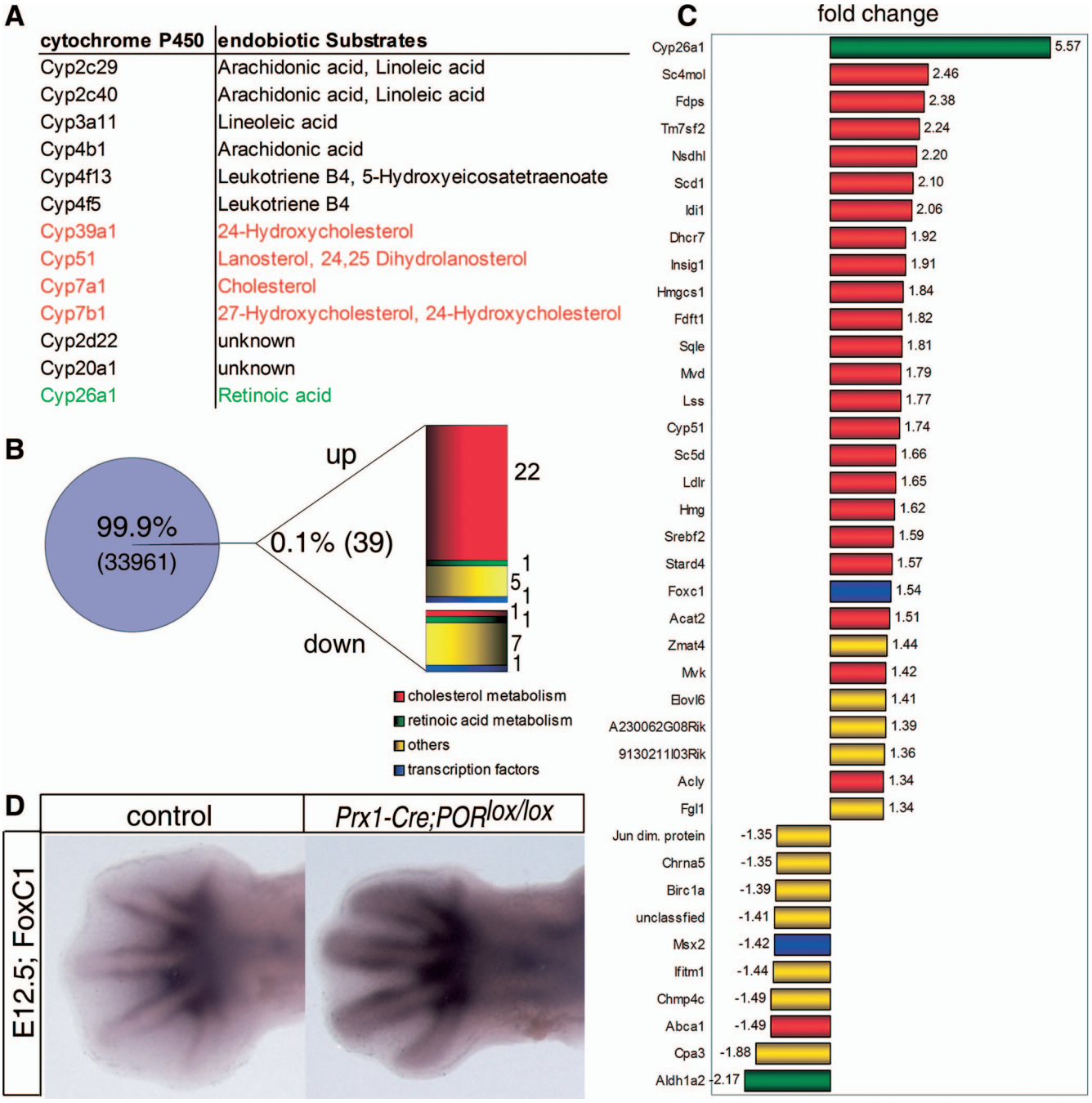

FIG. 7. Microarray analysis of E12.5 forelimb buds. (A) Transcripts of P450 enzymes in control embryos. The table shows all annotated Cyps with present calls (detection call above background) in all five arrays, together with the substrate specificities (according to the KEGG database). (B) Differentially expressed genes. All statistically significant probe sets with low false discovery rates represent 39 differentially expressed genes (0.1% of all genes on array). Genes involved in cholesterol homeostasis (red), retinoic acid-metabolizing enzymes (green), transcription factors (blue), and unknown transcripts or genes of unclassified function (yellow). The largest group (22) of upregulated genes in CKO samples is involved in cholesterol biosynthesis. (C) Changes of each differentially expressed gene, given next to each bar. Color coding as in panel B. Upregulation of cholesterol biosynthesis pathway indicates cholesterol deficiency through metabolic feedback. (D) In situ hybridization for *FoxC1*. The expression pattern confirms microarray results.

with the low-density lipoprotein receptor 1 (*LDLR1*) responsible for cholesterol uptake (6), *Stard4*, the protein participating in intracellular cholesterol transport, the sterol-sensing protein Insig1, and the sterol regulatory element binding factor 2 (*SREBP2*), while the gene encoding ATP-binding cassette A1 (*ABCA1*) involved in lipid efflux from cells (72) was downregulated (Fig. 9B; see Table S2 in the supplemental material). Furthermore, direct measurements of sterols made in E13.5 control and CKO limbs (Fig. 9C) showed that the amount of cholesterol per CKO limb bud was reduced compared to con-

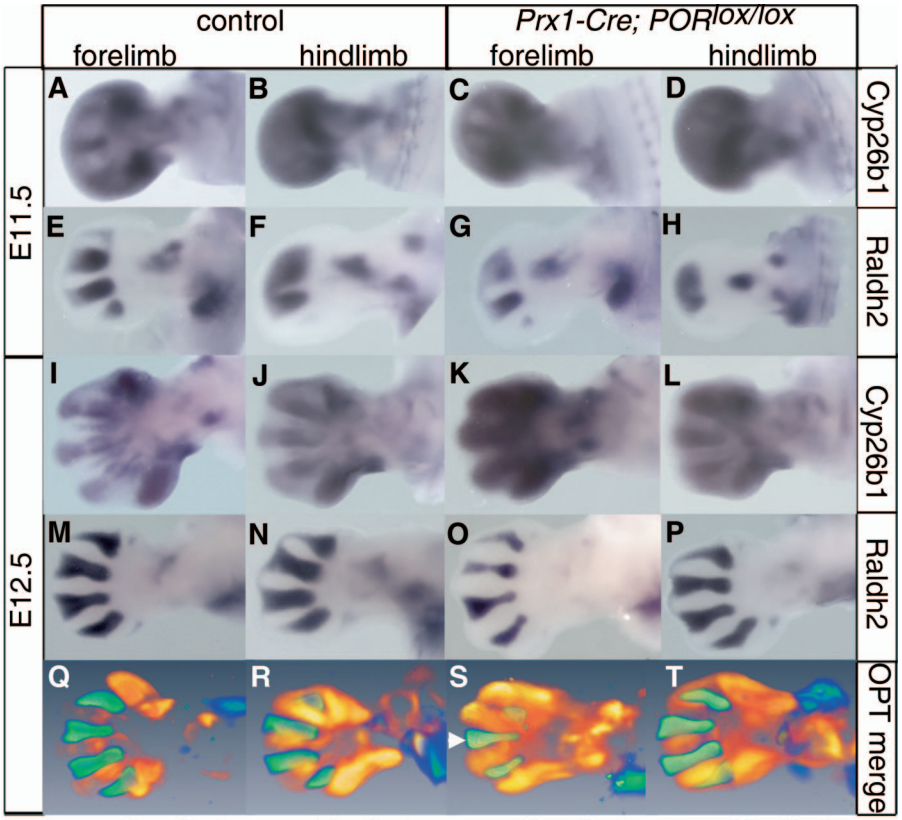

U	forelimb	hindlimb	forelimb	hindlimb
13cis RA [pg]	8.21	10.72	6.52	10.98
atRA [pg]	14.13	15.72	20.63	14.95
ROH [pg]	66.12	77.67	63.30	68 75
atRA/ ROH	**0.21±0.08**	**0.20±0.02**	**0.33±0.10**	**0.22±0.06**

FIG. 8. Retinoic acid homeostasis. (A to P) In situ hybridization for *Cyp26B1* (A to D and I to L) and *Raldh2* (E to H and M to P). Embryonic ages are indicated on the left, genotypes are indicated across the top, and riboprobes/methodology are indicated on the right. Hind limb buds were included as an internal control. Very little variation was seen. Note the accumulation of *Cyp26B1* transcripts in CKO forelimb buds at E12.5 (compare panels I and K) and the reduction of *Raldh2* transcripts (compare panels M and O); both findings are consistent with the microarray data (Fig. 7C). (Q to T) Optical projection tomography of E12.5 limb buds. *Cyp26B1* (orange) and *Raldh2* (green) expression patterns were digitally overlaid. Note that the interdigital space between digits 3 and 4 (white arrowhead) does not show overlapping expression of these two genes (S). (U) Quantification of atRA, retinol (ROH), and 13-*cis* retinoic acid (13cisRA) expressed as the mean per limb bud. Considerable variation was seen between samples for both genotypes, irrespective of whether the forelimb or hind limb was examined. Note that the mean value for atRA and the ratio of atRA/ROH (given as means ± the standard deviation) increased in CKO forelimbs but not hind limbs, a finding consistent with the expression patterns.

trol limb buds. Levels were lower in CKO forelimbs than in CKO hind limbs, showing that differential timing of *POR* deletion still has an effect at E13.5. These data show that POR inactivation led to cholesterol deficiency in CKO forelimbs. Further measurements in 2-month-old mice showed that, in CKO forelimbs, cholesterol was still reduced (87.3% in CKO mice compared to 92.9% in controls), whereas the precursor lathosterol had accumulated (12.7% for CKO mice versus 7.1% in controls), although the overall amounts of sterols were similar (CKO, 2.83 ± 0.36 mg of sterol extracted/g of extracted oil; control, 2.50 ± 0.54 mg/g).

We tried to rescue the forelimb phenotype by manipulating the diet of dams, feeding them either a VAD diet to counter retinoic acid excess, a diet supplemented with 2% cholesterol to counter cholesterol deficiency, or a combination of both diets. Examination of forelimbs of CKO embryos from dams on either cholesterol supplemented or combined diet showed that soft tissue webbing was less obvious particularly at E14.5 (Fig. 9D and data not shown [compare to Fig. 4F, inset]). In contrast, on a VAD diet, soft tissue webbing and splaying of digits 3 and 4 was still pronounced (data not shown). These data are consistent with the involvement of cholesterol deficiency in soft tissue syndactyly in CKO forelimbs.

DISCUSSION

We have shown that POR is required for normal development of the limb and its skeleton. *POR* deficiency in humans

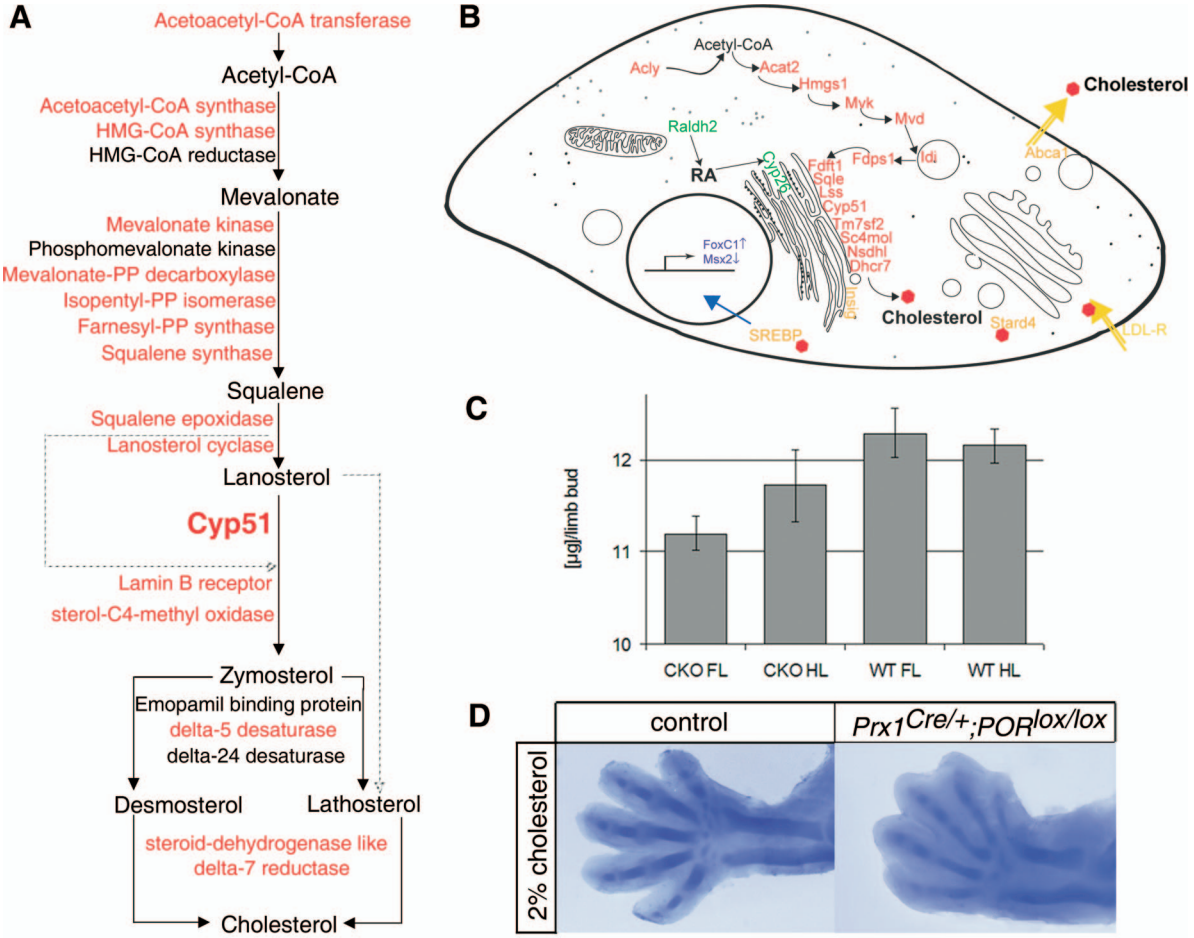

FIG. 9. Changes in metabolism in *Prx1-Cre*; $POR^{lox/lox}$ limb bud cells and levels of cholesterol. (A) Cholesterol biosynthesis pathway (see also Table S2 in the supplemental material). Upregulated enzymes in CKO forelimb buds are shown (red). Note that Cyp51 as a POR-dependent enzyme is nonfunctional despite being upregulated. (B) POR deficiency on a cellular level based on microarray results. Colors: cholesterol metabolic pathway, red; cholesterol, red hexagons; cholesterol transport, yellow; retinoic acid metabolic pathway, green; transcription factors, blue. (C) Cholesterol quantification in E13.5 limb buds. CKO forelimbs show reduced cholesterol levels compared to controls Values were calculated per limb bud and represent the mean of three embryos. (D) Rescue experiment. To try and rescue the phenotype, dams were given a diet enriched with 2% cholesterol. Embryos were prepared at E14.5 and stained for cartilage. Splaying between digits 3 and 4 was reduced (compare to Fig. 4F).

causes disordered steroidogenesis and occasionally bone malformations resembling Antley-Bixler syndrome (27). By knocking out *POR* specifically in limb bud mesenchyme in the embryo, we were able to reproduce most skeletal malformations seen in systemic *POR* deficiency seen in patients, such as abnormal bowing of long bones, joint contractures, ankylosis, and digital abnormalities (11, 34), with some of these features being more prominent postnatally. We saw some aspects such as digital abnormalities in only the forelimbs of CKO embryos although other features were seen in both forelimbs and hind limbs. The reason for this difference is that *POR* deletion occurs at an earlier stage in development and is more efficient in the forelimbs than in the hind limbs using *Prx-Cre*, as has been reported previously (49). Since the forelimb phenotype has more of the features seen in *POR* deficiency in human patients, we concentrated on analyzing the development of the forelimbs at the molecular level. Overall, our results demonstrate the importance of cellular metabolism and a local functioning P450 system in the limb throughout development.

P450 pathways operating in limb development. Our microarray data showed that the digital plate of the developing mouse forelimb expresses P450 enzymes participating in retinoic acid, cholesterol, and arachidonic acid metabolism in addition to metabolizing chemical compounds; expression of nine of these, involving the same metabolic pathways, was also detected in whole E11 mouse embryos by reverse transcription-PCR (13). It is known from many studies that retinoic acid metabolism and Cyp26 enzymes play major roles in embryogenesis, limb development, and patterning (52, 55, 61, 62, 70, 96), and the general relevance of cholesterol metabolism for embryogenesis has also been well established (42, 89). In contrast, although arachidonic acid metabolism is known to contain cytochrome P450-regulated steps (9, 10) and its products have been implicated in vascular homeostasis and angiogenesis (5, 26), little is known about the function of this pathway in embryonic development. Thus, although Cyp enzymes involved in arachidonic acid metabolism are expressed in the digital plate of the forelimb, it is not clear whether inactivation of this

pathway contributes to the defects. Some cytochrome P450s from the Cyp2 family have been highlighted as potentially interesting in a developmental context because they generate *cis*-epoxyeicosatrienoic acids, which regulate a range of cellular processes (78). Thus, for example, Cyp2c29, one of the P450s we found to be expressed in the digital plate of the forelimb, generates 14,15-*cis*-epoxyeicosatrienoic acid, which has been shown to release a potent mitogenic growth factor in epithelial cell lines (12).

The importance of P450-dependent pathways downstream of POR which metabolize retinoic acid and cholesterol was confirmed by our biochemical analyses in developing limbs. In CKO mouse forelimbs, POR protein was markedly reduced at E10.5 and may have already begun to impair activity of P450 enzymes. As a consequence, by E12.5 to E13.5, the retinoic acid levels were markedly increased in CKO forelimbs, while the cholesterol levels were decreased. In CKO hind limbs, POR protein was still just detectable at E11.5 and retinoic acid levels had not increased by E12.5 and, although cholesterol levels were lower in CKO hind limbs at E13.5 compared to wild-type limbs, this decrease was not as marked as in CKO forelimbs.

The microarrays of CKO forelimbs at E12.5 showed changes in the expression of a cohort of genes involved in both retinoic acid and cholesterol pathways. These expression changes are indicative of metabolic feedback loops being used in order to compensate for retinoic acid excess and cholesterol deficiency, respectively (19, 73). It is striking that a microarray performed on the brain tissue of a cholesterol-deficient mouse (88) resulted in an upregulation of genes involved in cholesterol synthesis and cellular uptake, as well as a downregulation of *Abca1* (sterol efflux), very much like our results. We also found *SREBP-2* to be upregulated, which directly induces transcription of genes involved in cholesterol synthesis and uptake (40).

Lipid metabolism, in particular sterol levels, continued to be disturbed during the postnatal life of CKO mice. Two-month-old CKO mice had accumulated substantial amounts of lipid in the forepaws and still showed an unbalanced ratio in sterols. This shows that local dysfunctional metabolism cannot be compensated for by an intact liver even after birth. Further investigations will be needed to clarify whether, and to what extent, these changes in the limbs of 2-month-old animals are a direct consequence of embryonic cholesterol deficiency.

Contribution of metabolic pathways to forelimb defects. Elevated retinoic acid levels might cause the stunted growth of the distal part of the forelimb in *POR*-deficient mice and contribute to the patterning defects in the wrist and digits. It has been well established that the effects of excess retinoic acid on proximo-distal patterning depend on the time of embryo exposure, with earlier exposure reducing proximal elements and later exposure reducing distal elements (47). If retinoic acid levels are continuously elevated from the very beginning, then all parts of the limb should be more or less equally affected, as, for example, by functionally inactivating the retinoic acid-metabolizing enzyme Cyp26b1 (96). Thus, the relatively late increase in retinoic acid in *Prx1-Cre*; $POR^{lox/lox}$ forelimbs seems consistent with defects in wrist and digits while the failure to rescue syndactyly with the VAD diet makes it unlikely that excess retinoic acid makes a significant contribution to this aspect of the phenotype. How retinoic acid might cause the patterning defects is not clear because, for example, no changes in *Hox* gene expression were seen even in clearly malformed limbs. It might be significant that the expression of *FoxC1*, a gene encoding a transcription factor, shown to be upregulated in CKO forelimb buds in our microarray experiment, was enhanced particularly in the wrist region, a site of one of these pattern defects. *FoxC1* has been shown to respond directly to retinoic acid (53), and changes in its expression have been reported in DiGeorge syndrome (95), which is associated with defects in retinoic acid homeostasis. Interestingly, *FoxC1* has been linked to skeletal development (68) and mesodermal cell fate choice (91), but since its function has not yet been studied in limb development its potential contribution to the phenotype will require further investigation.

Cholesterol deficiency is clearly implicated in soft tissue syndactyly and the defective development of skeletal primordia in CKO forelimbs. Thus, for example, drug-induced cholesterol deficiency in rats leads to remarkably similar defects, including a wide space between digits 3 and 4 and even down to changes in the detailed expression of genes such as *Ihh* in developing digits (32). The fact that a high-cholesterol diet only slightly ameliorated the phenotype of CKO mice may be explained by the difficulty of passing on the full amount of cholesterol from dam to embryo since cholesterol has to be actively transported via the placenta (92).

The proximate cause of syndactyly in CKO forelimbs appears to be the reduction of interdigital *Msx2* expression, as shown by in situ hybridization experiments and microarrays. *Msx2* normally coincides with interdigital apoptosis during limb development (24), but in *Prx1-Cre*; $POR^{lox/lox}$ limb buds it is reduced except between digits 3 and 4, although why this space is spared is not clear. Interestingly, enzymes of cholesterol biosynthesis are regionally restricted in their expression during normal digital morphogenesis, e.g., *HMG-CoA reductase* expression becomes confined to interdigital zones which undergo apoptosis at E12.5 (48).

The CKO limb phenotype has features in common with human syndromes known to be caused by mutations in cholesterol-synthesizing enzymes (37, 45, 85) and with the related mouse models, even though these are all systemic disorders, whereas our *Prx1-Cre*; $POR^{lox/lox}$ mice have a strictly peripheral deficiency. Thus, for example, patients with Smith-Lemli-Opitz Syndrome, caused by a mutation in *7-Dehydrocholesterol reductase*, often show 2,3 toe syndactyly in addition to postaxial polydactyly (17), while patients with mutations in either *Desmosterol reductase* (25), *Emopamil binding protein*, or *NADH steroid dehydrogenase-like* (CHILD syndrome or X-linked dominant chondrodysplasis punctata [38, 44]) or *Lamin B receptor* (90) have short limbs. In some cases, the related mouse model has no limb defects like the Desmosterolosis model but, in others, the mice have a wider range of limb abnormalities, including shortening, soft tissue syndactyly, and polydactyly (44, 89).

It has been proposed that the basis for limb defects seen under conditions of cholesterol deficiency is due to perturbation of Hedgehog signaling because cholesterol modification of Hedgehog proteins has been shown to affect signaling range and efficiency (reviewed in references 21, 30, and 50) and because Sonic hedgehog (Shh) and Indian hedgehog (Ihh) are critical for limb patterning and skeletogenesis (8, 87, 97).

Gofflot et al. (32) suggested that syndactyly of anterior digits in rat embryos after treatment with a cholesterol inhibitor arises because this part of the limb bud fails to expand normally due to changes in the range of Shh. However, in *Prx1-Cre*; $POR^{lox/lox}$ limb buds, there is syndactyly of both anterior and posterior digits, and the changes in cholesterol levels may occur too late to affect Shh signaling. Therefore, syndactyly may be due to perturbed Ihh activity, which would also explain the reduction in longitudinal growth of the skeletal elements in the limb (77). We examined the expression of two genes, *Patched1* and *Gli1*, which are known to be transcriptionally regulated by Hedgehog signaling and often used as reporters of hedgehog responding cells, in E13.5 forelimbs (see Fig. S1A to D in the supplemental material). Both expression patterns were slightly changed compared to control embryos, but this may be due to altered *Ihh* expression in CKO limbs (see Fig. 5H) rather than a change in the range of Ihh signaling.

It is intriguing that Hedgehog activity has been shown to be influenced by metabolites of all three P450 pathways (2, 16, 41, 94) identified in the limb and that alterations in retinoic acid, cholesterol, and arachidonic acid metabolism may all converge on Hedgehog signaling.

Implications. Through conditional *POR* deletion, we have identified three P450 pathways that operate in developing limb and skeleton. Uncovering these endogenous functions of P450s is critical in understanding embryonic metabolism and may also be relevant to teratogenesis. Thus, for example, it is well established that drugs and known teratogens such as polychlorinated biphenyls can alter P450 gene expression, and this could potentially lead to inappropriate distributions of developmentally active molecules in embryos (78). Following the suggestion about the basis for fetal alcohol syndrome (20), we speculate that some Cyp enzymes may have higher affinities for xenobiotic compounds than for their endogenous substrates. Thus, an excess of xenobiotic compounds during embryogenesis may keep the P450 system occupied and thereby distract it from metabolizing endogenous compounds. This could then lead to accumulation of endogenous substrates and deficiency of products, both of which could be manifested in disease or malformation.

ACKNOWLEDGMENTS

This study was supported by Wellcome Trust Project grant 072523 awarded to C.R.W. and C.T. C.T. is also funded by The Royal Society. C.H. and C.R.W. are also supported by Cancer Research UK (program grant C4639/A5661).

Skillful technical assistance with animal work by Dianne Carrie is gratefully acknowledged, as is the contribution of Leslie Dickman to initial stages of this study. We also thank Helen Downie for the 3D gene expression patterns and David FitzPatrick for valuable discussions.

REFERENCES

1. **Akiyama, H., M. C. Chaboissier, J. F. Martin, A. Schedl, and B. de Crombrugghe.** 2002. The transcription factor Sox9 has essential roles in successive steps of the chondrocyte differentiation pathway and is required for expression of Sox5 and Sox6. Genes Dev. **16:**2813–2828.
2. **Bijlsma, M. F., K. S. Borensztajn, H. Roelink, M. P. Peppelenbosch, and C. A. Spek.** 2007. Sonic hedgehog induces transcription-independent cytoskeletal rearrangement and migration regulated by arachidonate metabolites. Cell Signal. **19:**2596–2604.
3. **Black, S. D., and M. J. Coon.** 1987. P-450 cytochromes: structure and function. Adv. Enzymol. Relat. Areas Mol. Biol. **60:**35–87.
4. **Blomhoff, R., and H. K. Blomhoff.** 2006. Overview of retinoid metabolism and function. J. Neurobiol. **66:**606–630.
5. **Bogatcheva, N. V., M. G. Sergeeva, S. M. Dudek, and A. D. Verin.** 2005. Arachidonic acid cascade in endothelial pathobiology. Microvasc. Res. **69:** 107–127.
6. **Brown, M. S., and J. L. Goldstein.** 1986. A receptor-mediated pathway for cholesterol homeostasis. Science **232:**34–47.
7. **Campbell, S. J., C. J. Henderson, D. C. Anthony, D. Davidson, A. J. Clark, and C. R. Wolf.** 2005. The murine Cyp1a1 gene is expressed in a restricted spatial and temporal pattern during embryonic development. J. Biol. Chem. **280:**5828–5835.
8. **Capdevila, J., and R. L. Johnson.** 2000. Hedgehog signaling in vertebrate and invertebrate limb patterning. Cell Mol. Life Sci. **57:**1682–1694.
9. **Capdevila, J. H., J. R. Falck, and R. C. Harris.** 2000. Cytochrome P450 and arachidonic acid bioactivation: molecular and functional properties of the arachidonate monooxygenase. J. Lipid Res. **41:**163–181.
10. **Carroll, M. A., M. K. Cheng, E. L. Liclican, J. Li, A. B. Doumad, and J. C. McGiff.** 2005. Purinoceptors in renal microvessels: adenosine-activated and cytochrome P450 monooxygenase-derived arachidonate metabolites. Pharmacol. Rep. **57**(Suppl.)**:**191–195.
11. **Chabchoub, A., S. Siala-Gaigi, Z. Marrakchi, S. Jebnoun, R. Ayachi, and N. Khrouf.** 1998. The Antley-Bixler syndrome: a new case without radiohumeral synostosis. Genet. Couns. **9:**113–118.
12. **Chen, J. K., J. Capdevila, and R. C. Harris.** 2002. Heparin-binding EGF-like growth factor mediates the biological effects of P450 arachidonate epoxygenase metabolites in epithelial cells. Proc. Natl. Acad. Sci. USA **99:**6029–6034.
13. **Choudhary, D., I. Jansson, J. B. Schenkman, M. Sarfarazi, and I. Stoilov.** 2003. Comparative expression profiling of 40 mouse cytochrome P450 genes in embryonic and adult tissues. Arch. Biochem. Biophys. **414:**91–100.
14. **Choudhary, D., I. Jansson, I. Stoilov, M. Sarfarazi, and J. B. Schenkman.** 2005. Expression patterns of mouse and human CYP orthologs (families 1-4) during development and in different adult tissues. Arch. Biochem. Biophys. **436:**50–61.
15. **Cobb, J., A. Dierich, Y. Huss-Garcia, and D. Duboule.** 2006. A mouse model for human short-stature syndromes identifies Shox2 as an upstream regulator of Runx2 during long-bone development. Proc. Natl. Acad. Sci. USA **103:** 4511–4515.
16. **Cooper, M. K., J. A. Porter, K. E. Young, and P. A. Beachy.** 1998. Teratogen-mediated inhibition of target tissue response to Shh signaling. Science **280:** 1603–1607.
17. **Cunniff, C., L. E. Kratz, A. Moser, M. R. Natowicz, and R. I. Kelley.** 1997. Clinical and biochemical spectrum of patients with RSH/Smith-Lemli-Opitz syndrome and abnormal cholesterol metabolism. Am. J. Med. Genet. **68:** 263–269.
18. **Dahlquist, K. D., N. Salomonis, K. Vranizan, S. C. Lawlor, and B. R. Conklin.** 2002. GenMAPP, a new tool for viewing and analyzing microarray data on biological pathways. Nat. Genet. **31:**19–20.
19. **Dobbs-McAuliffe, B., Q. Zhao, and E. Linney.** 2004. Feedback mechanisms regulate retinoic acid production and degradation in the zebrafish embryo. Mech. Dev. **121:**339–350.
20. **Duester, G.** 1991. A hypothetical mechanism for fetal alcohol syndrome involving ethanol inhibition of retinoic acid synthesis at the alcohol dehydrogenase step. Alcohol Clin. Exp. Res. **15:**568–572.
21. **Eaton, S.** 2008. Multiple roles for lipids in the Hedgehog signalling pathway. Nat. Rev. Mol. Cell. Biol. **9:**437–445.
22. **Elima, K., I. Eerola, R. Rosati, M. Metsaranta, S. Garofalo, M. Perala, B. De Crombrugghe, and E. Vuorio.** 1993. The mouse collagen X gene: complete nucleotide sequence, exon structure and expression pattern. Biochem. J. **289**(Pt. 1)**:**247–253.
23. **Espenshade, P. J., and A. L. Hughes.** 2007. Regulation of sterol synthesis in eukaryotes. Annu. Rev. Genet. **41:**401–427.
24. **Ferrari, D., A. C. Lichtler, Z. Z. Pan, C. N. Dealy, W. B. Upholt, and R. A. Kosher.** 1998. Ectopic expression of Msx-2 in posterior limb bud mesoderm impairs limb morphogenesis while inducing BMP-4 expression, inhibiting cell proliferation, and promoting apoptosis. Dev. Biol. **197:**12–24.
25. **FitzPatrick, D. R., J. W. Keeling, M. J. Evans, A. E. Kan, J. E. Bell, M. E. Porteous, K. Mills, R. M. Winter, and P. T. Clayton.** 1998. Clinical phenotype of desmosterolosis. Am. J. Med. Genet. **75:**145–152.
26. **Fleming, I.** 2001. Cytochrome p450 and vascular homeostasis. Circ. Res. **89:**753–762.
27. **Fluck, C. E., T. Tajima, A. V. Pandey, W. Arlt, K. Okuhara, C. F. Verge, E. W. Jabs, B. B. Mendonca, K. Fujieda, and W. L. Miller.** 2004. Mutant P450 oxidoreductase causes disordered steroidogenesis with or without Antley-Bixler syndrome. Nat. Genet. **36:**228–230.
28. **Folch, J., M. Lees, and G. H. Sloane Stanley.** 1957. A simple method for the isolation and purification of total lipids from animal tissues. J. Biol. Chem. **226:**497–509.
29. **Fukami, M., R. Horikawa, T. Nagai, T. Tanaka, Y. Naiki, N. Sato, T. Okuyama, H. Nakai, S. Soneda, K. Tachibana, N. Matsuo, S. Sato, K. Homma, G. Nishimura, T. Hasegawa, and T. Ogata.** 2005. Cytochrome P450 oxidoreductase gene mutations and Antley-Bixler syndrome with abnormal genitalia and/or impaired steroidogenesis: molecular and clinical studies in 10 patients. J. Clin. Endocrinol. Metab. **90:**414–426.
30. **Gallet, A., L. Ruel, L. Staccini-Lavenant, and P. P. Therond.** 2006. Choles-

terol modification is necessary for controlled planar long-range activity of Hedgehog in *Drosophila* epithelia. Development **133:**407–418.
31. **Gentleman, R. C., V. J. Carey, D. M. Bates, B. Bolstad, M. Dettling, S. Dudoit, B. Ellis, L. Gautier, Y. Ge, J. Gentry, K. Hornik, T. Hothorn, W. Huber, S. Iacus, R. Irizarry, F. Leisch, C. Li, M. Maechler, A. J. Rossini, G. Sawitzki, C. Smith, G. Smyth, L. Tierney, J. Y. Yang, and J. Zhang.** 2004. Bioconductor: open software development for computational biology and bioinformatics. Genome Biol. **5:**R80.
32. **Gofflot, F., C. Hars, F. Illien, F. Chevy, C. Wolf, J. J. Picard, and C. Roux.** 2003. Molecular mechanisms underlying limb anomalies associated with cholesterol deficiency during gestation: implications of Hedgehog signaling. Hum. Mol. Genet. **12:**1187–1198.
33. **Gundersen, T. E., N. E. Bastani, and R. Blomhoff.** 2007. Quantitative high-throughput determination of endogenous retinoids in human plasma using triple-stage liquid chromatography/tandem mass spectrometry. Rapid Commun. Mass Spectrom. **21:**1176–1186.
34. **Hassell, S., and M. G. Butler.** 1994. Antley-Bixler syndrome: report of a patient and review of literature. Clin. Genet. **46:**372–376.
35. **Henderson, C. J., D. M. Otto, D. Carrie, M. A. Magnuson, A. W. McLaren, I. Rosewell, and C. R. Wolf.** 2003. Inactivation of the hepatic cytochrome P450 system by conditional deletion of hepatic cytochrome P450 reductase. J. Biol. Chem. **278:**13480–13486.
36. **Henderson, C. J., G. J. Pass, and C. R. Wolf.** 2006. The hepatic cytochrome P450 reductase null mouse as a tool to identify a successful candidate entity. Toxicol. Lett. **162:**111–117.
37. **Herman, G. E.** 2003. Disorders of cholesterol biosynthesis: prototypic metabolic malformation syndromes. Hum. Mol. Genet. **12**(Spec. No. 1)**:**R75–R88.
38. **Herman, G. E.** 2000. X-Linked dominant disorders of cholesterol biosynthesis in man and mouse. Biochim. Biophys. Acta **1529:**357–373.
39. **Hernandez, R. E., A. P. Putzke, J. P. Myers, L. Margaretha, and C. B. Moens.** 2007. Cyp26 enzymes generate the retinoic acid response pattern necessary for hindbrain development. Development **134:**177–187.
40. **Horton, J. D., N. A. Shah, J. A. Warrington, N. N. Anderson, S. W. Park, M. S. Brown, and J. L. Goldstein.** 2003. Combined analysis of oligonucleotide microarray data from transgenic and knockout mice identifies direct SREBP target genes. Proc. Natl. Acad. Sci. USA **100:**12027–12032.
41. **Huq, M. D., N. P. Tsai, P. Gupta, and L. N. Wei.** 2006. Regulation of retinal dehydrogenases and retinoic acid synthesis by cholesterol metabolites. EMBO J. **25:**3203–3213.
42. **Javitt, N. B.** 2007. Oxysterols: functional significance in fetal development and the maintenance of normal retinal function. Curr. Opin. Lipidol. **18:** 283–288.
43. **Keeney, D. S., and M. R. Waterman.** 1999. Two novel sites of expression of NADPH cytochrome P450 reductase during murine embryogenesis: limb mesenchyme and developing olfactory neuroepithelia. Dev. Dyn. **216:**511–517.
44. **Kelley, R. I., and G. E. Herman.** 2001. Inborn errors of sterol biosynthesis. Annu. Rev. Genomics Hum. Genet. **2:**299–341.
45. **Krakowiak, P. A., C. A. Wassif, L. Kratz, D. Cozma, M. Kovarova, G. Harris, A. Grinberg, Y. Yang, A. G. Hunter, M. Tsokos, R. I. Kelley, and F. D. Porter.** 2003. Lathosterolosis: an inborn error of human and murine cholesterol synthesis due to lathosterol 5-desaturase deficiency. Hum. Mol. Genet. **12:** 1631–1641.
46. **Kume, T., K. Y. Deng, V. Winfrey, D. B. Gould, M. A. Walter, and B. L. Hogan.** 1998. The forkhead/winged helix gene Mf1 is disrupted in the pleiotropic mouse mutation congenital hydrocephalus. Cell **93:**985–996.
47. **Kwasigroch, T. E., J. F. Vannoy, J. K. Church, and R. G. Skalko.** 1986. Retinoic acid enhances and depresses in vitro development of cartilaginous bone anlagen in embryonic mouse limbs. In Vitro Cell Dev. Biol. **22:**150–156.
48. **Laubner, D., R. Breitling, and J. Adamski.** 2003. Embryonic expression of cholesterogenic genes is restricted to distinct domains and colocalizes with apoptotic regions in mice. Brain Res. Mol. Brain Res. **115:**87–92.
49. **Lee, C. T., L. Li, N. Takamoto, J. F. Martin, F. J. Demayo, M. J. Tsai, and S. Y. Tsai.** 2004. The nuclear orphan receptor COUP-TFII is required for limb and skeletal muscle development. Mol. Cell. Biol. **24:**10835–10843.
50. **Li, Y. X., H. T. Yang, M. Zdanowicz, J. K. Sicklick, Y. Qi, T. J. Camp, and A. M. Diehl.** 2007. Fetal alcohol exposure impairs Hedgehog cholesterol modification and signaling. Lab. Investig. **87:**231–240.
51. **Logan, M., J. F. Martin, A. Nagy, C. Lobe, E. N. Olson, and C. J. Tabin.** 2002. Expression of Cre recombinase in the developing mouse limb bud driven by a Prxl enhancer. Genesis **33:**77–80.
52. **Maden, M.** 2000. The role of retinoic acid in embryonic and post-embryonic development. Proc. Nutr. Soc. **59:**65–73.
53. **Matt, N., V. Dupe, J. M. Garnier, C. Dennefeld, P. Chambon, M. Mark, and N. B. Ghyselinck.** 2005. Retinoic acid-dependent eye morphogenesis is orchestrated by neural crest cells. Development **132:**4789–4800.
54. **McLeod, M. J.** 1980. Differential staining of cartilage and bone in whole mouse fetuses by Alcian Blue and Alizarin Red S. Teratology **22:**299–301.
55. **Mic, F. A., A. Molotkov, N. Molotkova, and G. Duester.** 2004. Raldh2 expression in optic vesicle generates a retinoic acid signal needed for invagination of retina during optic cup formation. Dev. Dyn. **231:**270–277.
56. **Miller, W. L.** 2005. Minireview: regulation of steroidogenesis by electron transfer. Endocrinology **146:**2544–2550.
57. **Nebert, D. W., and D. W. Russell.** 2002. Clinical importance of the cytochromes P450. Lancet **360:**1155–1162.
58. **Nelson, D. R.** 1999. Cytochrome P450 and the individuality of species. Arch. Biochem. Biophys. **369:**1–10.
59. **Nelson, D. R., D. C. Zeldin, S. M. Hoffman, L. J. Maltais, H. M. Wain, and D. W. Nebert.** 2004. Comparison of cytochrome P450 (CYP) genes from the mouse and human genomes, including nomenclature recommendations for genes, pseudogenes, and alternative-splice variants. Pharmacogenetics **14:**1–18.
60. **Ng, L. J., P. P. Tam, and K. S. Cheah.** 1993. Preferential expression of alternatively spliced mRNAs encoding type II procollagen with a cysteine-rich amino-propeptide in differentiating cartilage and nonchondrogenic tissues during early mouse development. Dev. Biol. **159:**403–417.
61. **Niederreither, K., V. Subbarayan, P. Dolle, and P. Chambon.** 1999. Embryonic retinoic acid synthesis is essential for early mouse post-implantation development. Nat. Genet. **21:**444–448.
62. **Niederreither, K., J. Vermot, B. Schuhbaur, P. Chambon, and P. Dolle.** 2002. Embryonic retinoic acid synthesis is required for forelimb growth and anteroposterior patterning in the mouse. Development **129:**3563–3574.
63. **Omura, T.** 1999. Forty years of cytochrome P450. Biochem. Biophys. Res. Commun. **266:**690–698.
64. **Otto, D. M., C. J. Henderson, D. Carrie, M. Davey, T. E. Gundersen, R. Blomhoff, R. H. Adams, C. Tickle, and C. R. Wolf.** 2003. Identification of novel roles of the cytochrome p450 system in early embryogenesis: effects on vasculogenesis and retinoic acid homeostasis. Mol. Cell. Biol. **23:**6103–6116.
65. **Pikuleva, I. A.** 2006. Cholesterol-metabolizing cytochromes P450. Drug Metab. Dispos. **34:**513–520.
66. **Reijntjes, S., A. Blentic, E. Gale, and M. Maden.** 2005. The control of morphogen signalling: regulation of the synthesis and catabolism of retinoic acid in the developing embryo. Dev. Biol. **285:**224–237.
67. **Ribes, V., D. M. Otto, L. Dickmann, K. Schmidt, B. Schuhbaur, C. Henderson, R. Blomhoff, C. R. Wolf, C. Tickle, and P. Dolle.** 2007. Rescue of cytochrome P450 oxidoreductase (Por) mouse mutants reveals functions in vasculogenesis, brain and limb patterning linked to retinoic acid homeostasis. Dev. Biol. **303:**66–81.
68. **Rice, R., D. P. Rice, B. R. Olsen, and I. Thesleff.** 2003. Progression of calvarial bone development requires Foxc1 regulation of Msx2 and Alx4. Dev. Biol. **262:**75–87.
69. **Roux, C., C. Wolf, N. Mulliez, W. Gaoua, V. Cormier, F. Chevy, and D. Citadelle.** 2000. Role of cholesterol in embryonic development. Am. J. Clin. Nutr. **71:**1270S–1279S.
70. **Sakai, Y., C. Meno, H. Fujii, J. Nishino, H. Shiratori, Y. Saijoh, J. Rossant, and H. Hamada.** 2001. The retinoic acid-inactivating enzyme CYP26 is essential for establishing an uneven distribution of retinoic acid along the anterio-posterior axis within the mouse embryo. Genes Dev. **15:**213–225.
71. **Salas-Vidal, E., C. Valencia, and L. Covarrubias.** 2001. Differential tissue growth and patterns of cell death in mouse limb autopod morphogenesis. Dev. Dyn. **220:**295–306.
72. **Schmitz, G., and T. Langmann.** 2001. Structure, function and regulation of the ABC1 gene product. Curr. Opin. Lipidol. **12:**129–140.
73. **Schoenheimer, R., and F. Breusch.** 1933. Synthesis and destruction of cholesterol in the organism. J. Biol. Chem. **103:**439–448.
74. **Sharpe, J., U. Ahlgren, P. Perry, B. Hill, A. Ross, J. Hecksher-Sorensen, R. Baldock, and D. Davidson.** 2002. Optical projection tomography as a tool for 3D microscopy and gene expression studies. Science **296:**541–545.
75. **Shen, A. L., K. A. O'Leary, and C. B. Kasper.** 2002. Association of multiple developmental defects and embryonic lethality with loss of microsomal NADPH-cytochrome P450 oxidoreductase. J. Biol. Chem. **277:**6536–6541.
76. **Smyth, G. K.** 2004. Linear models and empirical bayes methods for assessing differential expression in microarray experiments. Stat Appl. Genet. Mol. Biol. **3:**Article3.
77. **St-Jacques, B., M. Hammerschmidt, and A. P. McMahon.** 1999. Indian hedgehog signaling regulates proliferation and differentiation of chondrocytes and is essential for bone formation. Genes Dev. **13:**2072–2086.
78. **Stoilov, I.** 2001. Cytochrome P450s: coupling development and environment. Trends Genet. **17:**629–632.
79. **Storm, E. E., and D. M. Kingsley.** 1999. GDF5 coordinates bone and joint formation during digit development. Dev. Biol. **209:**11–27.
80. **Storm, E. E., and D. M. Kingsley.** 1996. Joint patterning defects caused by single and double mutations in members of the bone morphogenetic protein (BMP) family. Development **122:**3969–3979.
81. **Stromstedt, M., D. S. Keeney, M. R. Waterman, B. C. Paria, A. J. Conley, and S. K. Dey.** 1996. Preimplantation mouse blastocysts fail to express CYP genes required for estrogen biosynthesis. Mol. Reprod. Dev. **43:**428–436.
82. **Suzuki, T., J. Takeuchi, K. Koshiba-Takeuchi, and T. Ogura.** 2004. Tbx genes specify posterior digit identity through Shh and BMP signaling. Dev. Cell **6:**43–53.
83. **Swindell, E. C., C. Thaller, S. Sockanathan, M. Petkovich, T. M. Jessell, and G. Eichele.** 1999. Complementary domains of retinoic acid production and degradation in the early chick embryo. Dev. Biol. **216:**282–296.

84. **Tarchini, B., T. H. Huynh, G. A. Cox, and D. Duboule.** 2005. HoxD cluster scanning deletions identify multiple defects leading to paralysis in the mouse mutant Ironside. Genes Dev. **19:**2862–2876.
85. **Tozawa, R., S. Ishibashi, J. Osuga, H. Yagyu, T. Oka, Z. Chen, K. Ohashi, S. Perrey, F. Shionoiri, N. Yahagi, K. Harada, T. Gotoda, Y. Yazaki, and N. Yamada.** 1999. Embryonic lethality and defective neural tube closure in mice lacking squalene synthase. J. Biol. Chem. **274:**30843–30848.
86. **Tumpel, S., J. J. Sanz-Ezquerro, A. Isaac, M. C. Eblaghie, J. Dobson, and C. Tickle.** 2002. Regulation of Tbx3 expression by anteroposterior signalling in vertebrate limb development. Dev. Biol. **250:**251–262.
87. **Vortkamp, A., K. Lee, B. Lanske, G. V. Segre, H. M. Kronenberg, and C. J. Tabin.** 1996. Regulation of rate of cartilage differentiation by Indian hedgehog and PTH-related protein. Science **273:**613–622.
88. **Waage-Baudet, H., W. C. Dunty, Jr., D. B. Dehart, S. Hiller, and K. K. Sulik.** 2005. Immunohistochemical and microarray analyses of a mouse model for the Smith-Lemli-Opitz syndrome. Dev. Neurosci. **27:**378–396.
89. **Waterham, H. R.** 2002. Inherited disorders of cholesterol biosynthesis. Clin. Genet. **61:**393–403.
90. **Waterham, H. R., J. Koster, P. Mooyer, G. Noort Gv, R. I. Kelley, W. R. Wilcox, R. J. Wanders, R. C. Hennekam, and J. C. Oosterwijk.** 2003. Autosomal recessive HEM/Greenberg skeletal dysplasia is caused by 3 beta-hydroxysterol delta 14-reductase deficiency due to mutations in the lamin B receptor gene. Am. J. Hum. Genet. **72:**1013–1017.
91. **Wilm, B., R. G. James, T. M. Schultheiss, and B. L. Hogan.** 2004. The forkhead genes, *Foxc1* and *Foxc2*, regulate paraxial versus intermediate mesoderm cell fate. Dev. Biol. **271:**176–189.
92. **Woollett, L. A.** 2005. Maternal cholesterol in fetal development: transport of cholesterol from the maternal to the fetal circulation. Am. J. Clin. Nutr. **82:**1155–1161.
93. **Wright, E., M. R. Hargrave, J. Christiansen, L. Cooper, J. Kun, T. Evans, U. Gangadharan, A. Greenfield, and P. Koopman.** 1995. The Sry-related gene Sox9 is expressed during chondrogenesis in mouse embryos. Nat. Genet. **9:**15–20.
94. **Wu, L. N., M. Lu, B. R. Genge, G. Y. Guo, D. Nie, and R. E. Wuthier.** 2002. Discovery of sonic hedgehog expression in postnatal growth plate chondrocytes: differential regulation of sonic and Indian hedgehog by retinoic acid. J. Cell Biochem. **87:**173–187.
95. **Yamagishi, H., J. Maeda, T. Hu, J. McAnally, S. J. Conway, T. Kume, E. N. Meyers, C. Yamagishi, and D. Srivastava.** 2003. Tbx1 is regulated by tissue-specific forkhead proteins through a common Sonic hedgehog-responsive enhancer. Genes Dev. **17:**269–281.
96. **Yashiro, K., X. Zhao, M. Uehara, K. Yamashita, M. Nishijima, J. Nishino, Y. Saijoh, Y. Sakai, and H. Hamada.** 2004. Regulation of retinoic acid distribution is required for proximodistal patterning and outgrowth of the developing mouse limb. Dev. Cell **6:**411–422.
97. **Young, B., N. Minugh-Purvis, T. Shimo, B. St-Jacques, M. Iwamoto, M. Enomoto-Iwamoto, E. Koyama, and M. Pacifici.** 2006. Indian and sonic hedgehogs regulate synchondrosis growth plate and cranial base development and function. Dev. Biol. **299:**272–282.
98. **Zakany, J., C. Fromental-Ramain, X. Warot, and D. Duboule.** 1997. Regulation of number and size of digits by posterior Hox genes: a dose-dependent mechanism with potential evolutionary implications. Proc. Natl. Acad. Sci. USA **94:**13695–13700.
99. **Zakany, J., M. Kmita, and D. Duboule.** 2004. A dual role for Hox genes in limb anterior-posterior asymmetry. Science **304:**1669–1672.